COMMUNICATIONS IN SCIENCE AND TECHNOLOGY
Homepage: cst.kipmi.or.id

Synthesis of cellulose acetate (CA) from algae *Gracilaria sp.* composited with nickel oxide (NiO) as a supercapacitor base material

I Wayan Risdianto[a,*], Ahyar Ahmad[a], Riksfardini Annisa Ermawar[b]

[a]*Department of Chemistry, Faculty of Mathematics and Natural Science, Universitas Hasanuddin, Makassar 90245, Indonesia*
[b]*Pusat Riset Biomassa dan Bioproduk BRIN, Cibinong 16915, Indonesia*

Article history:
Received: 7 April 2023 / Received in revised form: 21 June 2023 / Accepted: 22 June 2023

Abstract

In this research, electrodes were made from cellulose acetate (CA) synthesized from algae *Gracilaria sp.* and then composited with nickel oxide (NiO), the concentration of which varied from 0, 0.2, 0.4, and 0.6 grams. Furthermore, FT-IR characterized cellulose acetate, and the CA-NiOn electrode was characterized by XRD, SEM, and cyclic voltammetry (CV). The results showed that CA was successfully synthesized from *Gracilaria sp.* Increasing the concentration of NiO added to CA as an electrode could increase the specific capacity, energy density, and power density of the electrode with the highest degree of 83.27 F/g, energy density of 4 Wh/kg, and a power density of 0.4 W/kg at a concentration of 0.6 gram NiO. The effect of the addition of NiO on the characteristics of the CA-NiOn electrode was also studied such as crystallinity, crystal size, and porosity. The presentation of CA doped with NiO has the promising prospects as a supercapacitor base material.

Keywords: Synthesis; Gracilaria Sp; Cellulose Acetate (CA); nickel oxide (NiO); supercapacitor

1. Introduction

Electrical energy in today's modern life has become a major necessity in human life [1]; this then drives the consumption of fossil fuels so that it has an impact on the increasing environmental pollution [2]. Batteries as an energy storage technology can reduce the use of fossil fuels, but storms have a relatively small power density, require quite a long time to charge, and are heavy, easily heated, and toxic [3]. Supercapacitors as an energy storage technology can be a solution for having advantages over batteries: high energy density, high-temperature resistance, fast charging, and environmental friendliness [4].

Cellulose acetate (CA) can be a promising alternative for manufacturing supercapacitors as efficient energy storage as it has a number of unique characteristics in terms of power and longevity and being environmentally friendly [5]. *Gracilaria sp.* as a source of cellulose can be synthesized into cellulose acetate [6]. Seaweed for industrial purposes is widely used to make semi-finished products such as agar powder and carrageenan flour [7]. One of the uses of seaweed in the industry is to produce solid waste, which still contains around 26.12% cellulose [8], which can later be further synthesized into cellulose acetate.

Research on supercapacitors based on the natural polymer cellulose acetate showed a potential as an energy storage material due to the ionic conductivity of the polar group, which had unpaired electrons but still exhibited a low specific capacitance as an electrode material [9].

Nickel oxide (NiO) is the most studied electrode due to its abundance, high capacitance, and low toxicity [10]. The addition of metal oxides to the cellulose acetate composite electrode film showed a change in structure and morphology. Meanwhile, the addition of metal oxides to the electrode film showed an increase of the surface area and the mobility of electrons enabling them to store energy [11].

Research on nickel oxide as an additional material for supercapacitor electrodes has also been studied and showed a high specific capacity. Al Kiey et al. [12] added nickel oxide to porous carbon fiber, increasing the specific capacity of 811 F/g at a current density of 1 A/g. Navale et al. [13] added nickel oxide to PANI and it increased the exact degree of 936 F/g at a current density of 1 A/g. Furthermore, Nunes et al. [14] added nickel oxide to carbon nanotubes and it increased the specific capacity of 1200 F/g at a current density of 5 A/g. Wang et al. [15] added nickel oxide to graphemes later increasing the specific capacity of 766 F/g at a current density of 1 A/g. All showed that a mixture of nickel oxide has the promising prospects as an additional material for supercapacitors.

Nickel oxide also has promising prospects as a base material for electrodes. However, research on cellulose acetate composited with nickel oxide as a supercapacitor electrode has never been carried out as an innovation. This research is expected to be an innovation in Blue Energy because it utilizes biomass waste from marine algae. It aims to study the potential of cellulose acetate, which is composited with nickel

* Corresponding author. Tel.: +62 82292962716
Email: risdyanto7.com@gmail.com
https://doi.org/10.21924/cst.8.1.2023.1176

oxide as a base material for high-capacity supercapacitor electrodes.

2. Materials and Methods

2.1. Materials and instrumen

This research phase began by synthesizing cellulose acetate from the algae *Gracilaria sp.* and then compositing it with nickel oxide (NiO) as the electrode supercapacitor material. The chemicals used in this study included sodium hydroxide (NaOH) 10% (w/v), hydrogen peroxide (H_2O_2) 30% (v/v), distilled water, glacial acetic acid (CH_3COOH), sulfuric acid (H_2SO_4) 2%, acetic anhydride ($(CH_3CO)_2O$), Sodium sulfate ($NaSO_4$) and dibutyl phthalate (DBP). The tools used in this research meanwhile included Fourier Transform Infrared (FT-IR) Shimadzu IR Prestige21 Europa, X-Ray Diffraction (XRD) Shimadzu XRD-7000L Germany, Scanning Electron Microscope (SEM) FEI Inspect-S50, and potentiostats EA161 for Cyclic Voltammetry analysis.

2.2. Preparation sample

Sample preparation of *Gracilaria sp.* started by separating algae *Gracilaria sp.* from the unwanted contaminants. *Gracilaria sp.* was then washed with running water, and dried in the sun before being ground into powder [16].

2.3. Cellulose insulation

Algae *Gracilaria sp.* has been made into dry powder in its cellulose isolation. Afterwards, 100 grams of 10% (w/v) sodium hydroxide (NaOH) was added to 1000 ml, and then heated at 90℃ to 100℃ for 3 hours before being filtered. The residue obtained was washed until making the pH of the filtrate neutral. The residue was then bleached by sequentially adding 50 ml of 30% (v/v) H_2O_2, heating it at 60℃ for 1 hour, and filtering. Subsequently, the filtered residue was dried in an oven at 60℃ [17]. FT-IR was then analyzed the dry solids were obtained.

2.4. Cellulose acetate synthesis

The isolated cellulose was further synthesized into cellulose acetate. Five grams of cellulose was added to 50 ml of the glacial acetic acid solution, and heated at 40°C for 60 minutes while stirring. 0.5 ml of 2% H2SO4 solution was again added and heated at 40°C for 60 minutes while stirring. 15 ml of acetic anhydride was added, and heated at 40°C for 30 minutes while stirring. Furthermore, 4 ml of distilled water and 7 ml of glacial acetic acid were added and heated at 40°C for 30 minutes while stirring. Another 160 ml of distilled water was added and allowed to stand for 2 hours prior to be filtered. The filtered residue was washed with distilled water until the sour smell disappeared and the pH became neutral. The residue was then dried in an oven at 55°C [18]. FT-IR then analyzed the dry solids obtained.

2.5. Electrode fabrication

In this study, variations in the concentration of nickel oxide were carried out on the electrode materials as shown in Table 1. 4 mL of dibutyl phthalate (DBP) was added. The mixture was then stirred at 250 rpm until being homogeneous at 80°C. The mixed solution was then poured into the mold [11]. SEM then analyzed the printouts to see the morphological structure, XRD to see the crystal structure, and tested with the cyclic voltammetry (CV) method to see the electrochemical properties of the electrodes.

Table 1. Variation of electrode material.

Sample code	Cellulose acetate (g)	Nickel oxide (g)	Total Mass(g)
CA-NiO_0	0.4	0	0.4
CA-NiO_1		0.2	0.6
CA-NiO_2	0.4	0.4	0.8
CA-NiO_3		0.6	1

3. Results and Discussion

3.1. FT-IR analysis of cellulose and CA

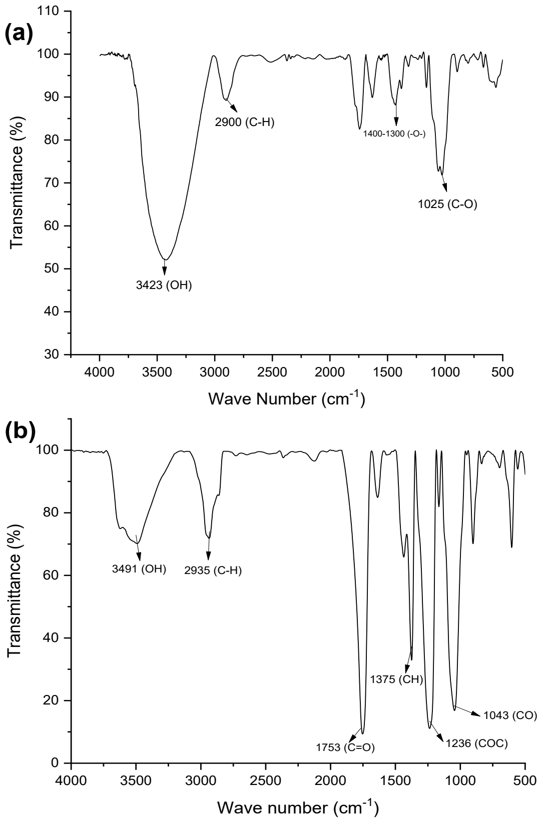

Fig. 1. (a). FT-IR cellulose isolation and (b). FT-IR cellulose acetate (CA).

Isolation aims to separate lignin from cellulose [19]. Lignin is undesirable because it can affect the acetylation reaction and the formation of the degree of substitution (DS) during further synthesis of cellulose into cellulose acetate [20]. As shown in Figure 1(a), a decrease in the intensity of the lignin band in the band in the range of 1500 cm^{-1} to 1,200 cm^{-1}, which was bound to the lignin carbonyl group occurred [21]. Figure 1(a) shows the absorption properties of cellulose at the intensity of wave number 3423 cm^{-1} (O-H) from the glycosidic bond while the (C-O) and ($-CH^2$) groups at 1026 cm^{-1} and 2900 cm^{-1} were cellulose ring regions [22] Several bands absorption at wave numbers 1300-1400 cm^{-1} indicated the presence of (-O-) connected to the carbon chain in cellulose [23].

Figure 1(b) shows the formation of an acetate group, which was confirmed by increasing intensity bands in 1753 cm^{-1} (C=O), 1236 cm^{-1} (C-O-O), and 1375 cm^{-1} (C-H) regions of the methyl group in acetate [9]. In the FT-IR spectrum, the hydroxyl groups (O-H) detected at an intensity of 3491 cm^{-1} had a lower level of peak state than the hydroxyl groups (O-H) in Figure 1(a). This indicated that most of the hydroxyl groups (O-H) originating from cellulose were replaced by acetate groups [24]. The lack of absorption in the 1840 cm^{-1} region in Figure 1(b) indicated that the product was free from acetic acid [25]. The success of the acetylation reaction was also proven in the formation of a carbonyl group (C=O) at an intensity of 1753 cm^{-1} and an acetyl group (C-O) at a power of 1043 cm^{-1} with a fairly high level of peak state.

3.2. XRD analysis

Electrode samples were characterized using XRD with a Cu Kα radiation source (λ = 1.5406 Å) at a voltage of 40 kV and a current of 30 mA. As shown in Figure 2, the mass variation diffraction of NiO added to CA showed the formation of CA-NiOn composites. It was established in the new peak of the CA-NiOn film when NiO was added. It was called as composite because there was a peak indicating 2 phases. These phases were CA as a matrix and NiO as a dopant. This is by research conducted by Diantoro et al. [11], where cellulose acetate doped with metal oxide will form composites.

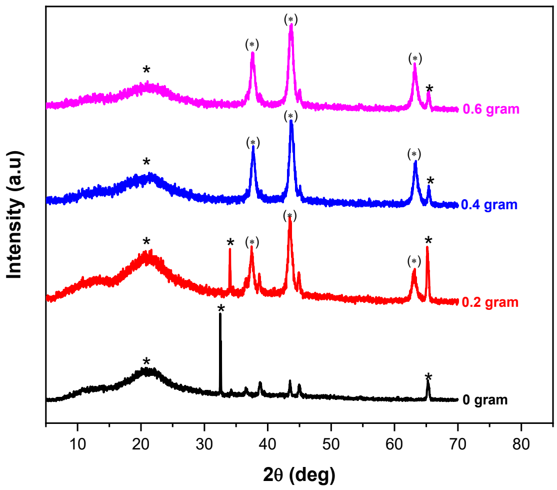

Fig. 2. Diffraction patterns of CA-NiO$_n$ composite electrodes for various concentrations of NiO, namely 0; 0.2; 0.4; and 0.6 grams. The symbols * and (*) are given for CA and NiO respectively.

All can be seen in Table 2 that the addition of NiO has increased the crystallinity of NiO and has decreased the crystallinity of CA, also seen in Figure 3 where the CA phase began to experience a decrease in peak intensity at position 2θ = 20°, 2θ = 32° and 2θ = 65° with the addition of NiO. The crystallinity of the CA-NiOn film was obtained using the following equation [26],

$$Crytallinity = (A_C / A_C + A_A) \times 100\% \quad (1)$$

where A_C is the crystalline area and A_A is the amorphous area.

Table 2. The crystallinity of CA and NiO of CA-NiO$_n$ electrodes.

Sample Code	Mass NiO (g)	Crystallinity (%)	
		CA	NiO
CA-NiO$_0$	0	70.97	0
CA-NiO$_1$	0.2	66.12	16.13
CA-NiO$_2$	0.4	58.69	28.48
CA-NiO$_3$	0.6	51.83	33.50

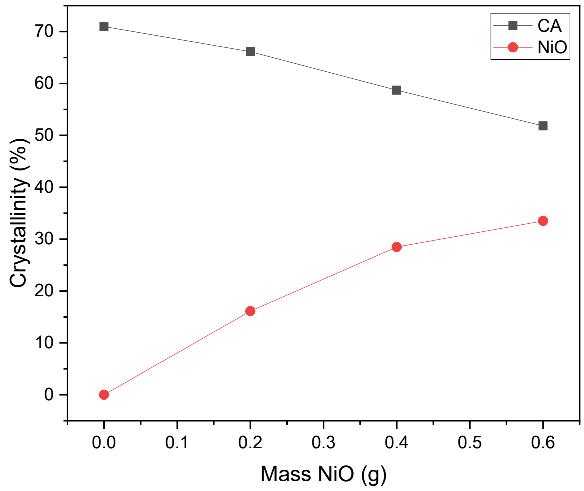

Fig. 3. The crystallinity of CA and NiO at various masses of NiO as CA-NiO$_n$ electrodes.

Table 3 shows the The crystal sizes of CA and NiO at the CA-NiOn electrodes are shown in Table 3. The crystal sizes could can be obtained using Equation 2 [26]. The crystal sizes of CA and NiO were about are around 3.82 – 30.8 nm and 7.93 – 31.22 nm, respectively. The data obtained based on the equation showeds a decrease in the size of CA crystals along with the addition of NiO. These results are the same as previous studies conducted by [27], where CA combined with metal oxides could can reduce the crystal size of CA. In Figure 4, it can be seen that there was a spike in the size of the NiO crystals . This is probably due to the higher concentration of NiO compared to CA.

$$D = k\,\lambda / \beta \cos\theta \quad (2)$$

where D is the crystal size, k is the crystal form factor, λ is the wavelength of Cu (1.54056 Å), β is the FWHM (rad), and θ is the diffraction angle (°).

Table 3. The Crystalsize of CA and NiO on mass variations of NiO on CA-NiO$_n$ electrodes.

Sample Code	Mass NiO (g)	Crystalsize (nm)	
		CA	NiO
CA-NiO$_0$	0	20.8	0
CA-NiO$_1$	0.2	5.11	7.93
CA-NiO$_2$	0.4	5.65	11.62
CA-NiO$_3$	0.6	3.82	31.22

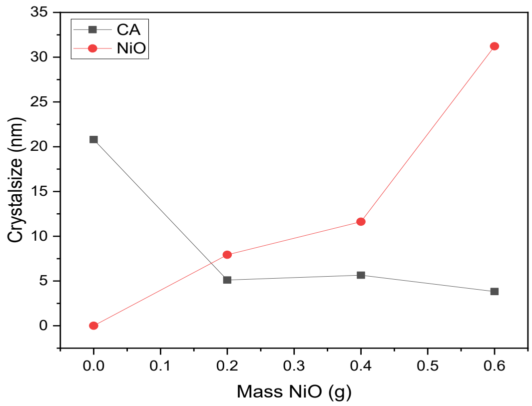

Fig. 4. The crystalsize of CA and NiO at various masses of NiO as CA-NiO_n electrodes.

3.3. SEM analysis

The SEM image showed that the CA-NiOn electrode was a porous film. The pores of the CA-NiOn electrode could be seen more clearly in 3D in Figure 6. Porosity is related to the capacity of the CA-NiOn electrode, which can decrease or increase, as shown in Figures 5 and 6 where the specific capacitance of the electrode increased with the increasing pore volume [28], and the porosity of the CA-NiOn electrode can be seen in Table 4. The porosity could be calculated using the following equation 3 [29],

$$Porous = \sum A_{Porous} / A_{total} \quad (3)$$

Where A is the area of the SEM results.

Table 4. Porous in CA-NiO_n electrode morphology.

Sample code	Mass NiO (g)	Porous (μm)
CA-NiO_0	0	0.62
CA-NiO_1	0.2	0.69
CA-NiO_2	0.4	0.72
CA-NiO_3	0.6	0.59

3.4. Electrochemical properties analysis of electrodes

It was tested in the voltage range from 0.0 to 1.0 V at a scanning speed of 10 mV/s. Specific capacitance (Csp), energy density (Esp), and power density (Psp) were calculated using standard equations based on cyclic voltammograms [30].

The addition of NiO decreased the crystallinity of the CA electrode film, as shown in Figure 2. The decrease in CA crystallinity significantly increased the specific capacity, energy density, and power density of the CA-NiOn electrode. This resulted from its molecules being more polarized under the influence of external fields [31]. Specific capacity, energy density, and power density were calculated using the following equation [32],

$$Csp = A / 2mk\,(V_2 - V_1) \quad (4)$$

$$Esp = 1/2\ Csp\,(\Delta V)^2 \quad (5)$$

$$Psp = Esp / \Delta t \quad (6)$$

where Csp is the specific capacity (F/g), Esp is the energy density (Wh/kg), Psp is the power density (kW/kg), A is the area of the curve, m is the mass of the electrode (grams), k is the scan rate (mV/s), V is voltage (V), and t is time (s).

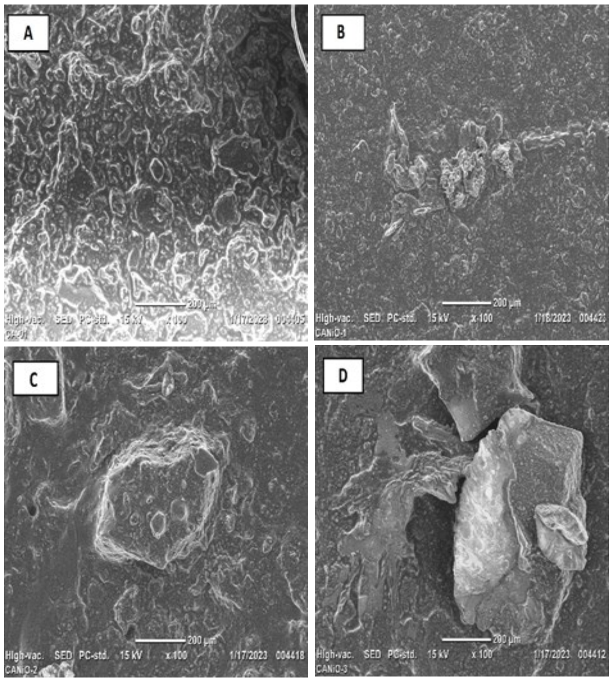

Fig. 5. Morphological structure (a) CA-NiO_0; (b) CA-NiO_1; (c) CA-NiO_2; (d) and CA-NiO_3

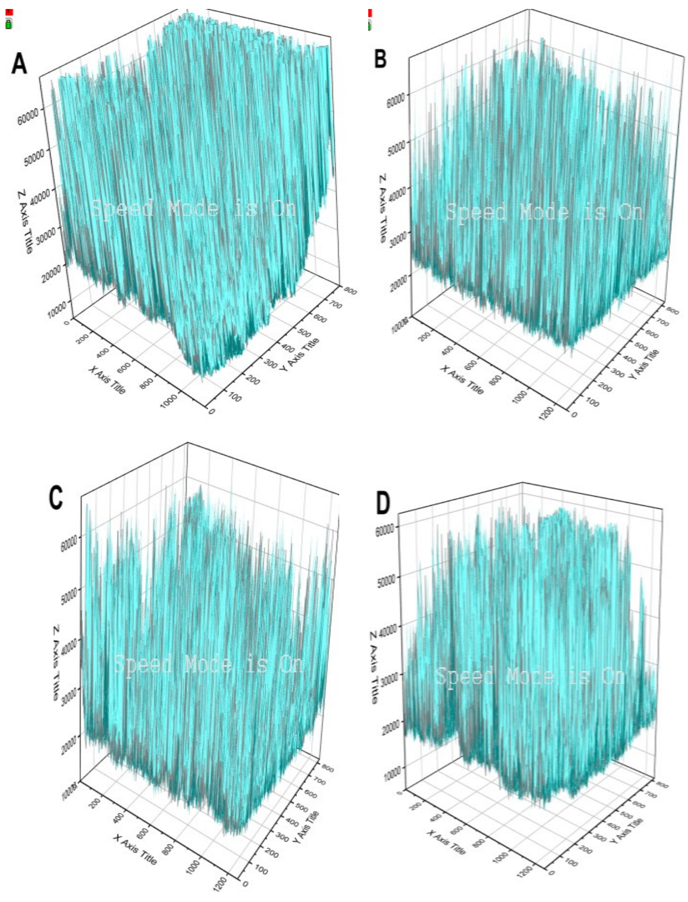

Fig. 6. Morphological structure (a) CA-NiO_0; (b) CA-NiO_1; (c) CA-NiO_2; (d) and CA-NiO_3, in three dimensions (3D).

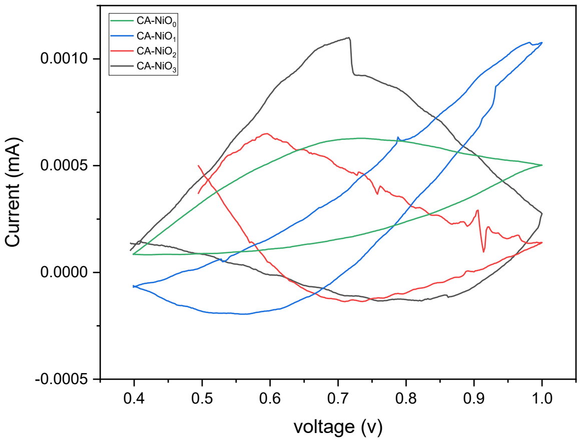

Fig. 7. CV curve of the CA-NiO$_n$ electrode with various masses of NiO.

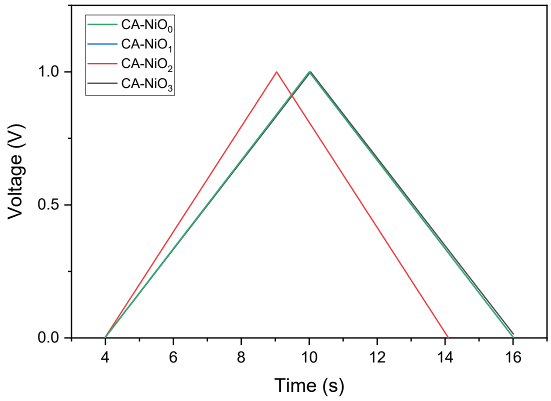

Fig. 8. CV curve of the CA-NiO$_n$ electrode

Gradually, the CV curve widened as the concentration of NiO in CA increased. This occurred since because the expanding the NiO engagement increased the electrode's capacity [33]. The specific capacitance could be evaluated based on the CV curve through the standard equation 4, which has been presented previously. Based on the equation, the specific capacitance was 14.25 F/g, 15.78 F/g, 26.24 F/g, and 83.27 F/g in which the CA-NiO$_3$ electrode had the highest specific capacity, followed by CA-NiO$_2$, CA-NiO$_1$, and CA-NiO$_0$, and the increase in particular capacity was followed by the increase in NiO concentration.

An increase in the specific capacity of the electrode affected the energy density and power density of the CA-NiOn electrode [34] where this value could be evaluated through standard equations 5 and 6. The data showed that an increase in the specific capacity could increase the electrodes' energy density and power density with energy density and power density values for each electrode CA-NiO$_0$, CA-NiO$_1$, CA-NiO$_2$, and CA-NiO$_3$, respectively 0.69 Wh/kg, 0.76 Wh/kg, 1.27 Wh/kg, and 4 Wh/ kg for energy density and 0.06 W/kg, 0.07 W/kg, 0.12 W/kg, and 0.4 W/kg for electrode power density. Based on the specific capacity value equation, the CV curve's power density and energy density can be seen more clearly in Table 4.

In the CV profile, the comparison between voltage and time in Figure 8 showed the shape of a symmetrical triangle curve, indicating the presence of promising electrical double-layer electrochemical capacitor properties in the sample [30]. The increase in specific capacity as the concentration of NiO increases indicated that NiO had an important role in increasing the power of the electrode.

Table 5. Specific capacitance (Csp), energy density (Esp), and density power (Psp) of the CV testing method.

Sample code	Csp (F/g)	Esp (Wh/kg)	Psp (W/kg)
CA-NiO$_0$	14.25	0.69	0.06
CA-NiO$_1$	15.78	0.76	0.07
CA-NiO$_2$	26.24	0.27	0.12
CA-NiO$_3$	83.22	4.0	0.4

4. Conclusion

Cellulose acetate has been successfully synthesized from the isolation of cellulose from the algae *Gracilaria sp.* as evidenced by FTIR spectral analysis. From the analysis of XRD data, the CA-NiOn electrode film was a composite film with CA and NiO crystal sizes of 3.82 – 30.8 nm and 7.93 – 31.22 nm, respectively. The results of the SEM analysis showed that the morphology of the CA-NiOn electrode included a porous film. In addition, increasing the concentration of NiO doped on the CA film could increase the specific capacity of the electrode with the highest capacity value of 83.27 F/g.

References

1. R. Asnawi, D. Nurhadiyanto, Z. Arifin, and A. Asmara, *The Characteristic of Supercapacitors Circuit as a Future Electrical Energy Storage Media*, J. Phys.: Conf. Ser. 1140 (2018), 012001.
2. Q. Cao, M. Zhu, J. Chen, Y. Song, Y. Li, and J. Zhou, *Novel Lignin-Cellulose Based Carbon Nanofibers as High-Performance Supercapacitors*, ACS Appl. Mater. Interfaces., (2019).
3. M. Wang, K. Liu, S. Dutta, D. S. Alessi, J. Rinklebe, Y. S. Ok, et al., *Recycling of lithium iron phosphate batteries: Status, technologies, challenges, and prospects*, Renew. Susta. Ener. Rev. Elsevier., 163(C), (2022).
4. K. Subasinghage, K. Gunawardane, N. Padmawansa, N. Kularatna, and M. Moradian, *Modern Supercapacitors Technologies and Their Applicability in Mature Electrical Engineering Applications*, J. Energ., 15 (2022), 7752.
5. G. E. Spina, F. Poli, A. Brilloni, D. Marchese, and F. Soavi, *Natural Polymers for Green Supercapacitors*, J. Energ., 13 (2020), 3115.
6. Z. Zhang, Z. Fang, Y. Xiang, D. Liu, Z. Xie, D. Qu, et al., *Cellulose-based material in lithium-sulfur batteries: A review*, J. Carbo. Polym., 255 (2021), 117469.
7. R. P. Juarsa, *Analisis dan Strategi untuk Mendukung Prospek Perdagangan Rumput Laut Indonesia*, J. Cen. Niag., 3 (2019), 4-7.
8. R. Battisti, E. Hafemann, C.A. Claumann, R.A.F. Machado, and C. Marangoni, *Synthesis and characterization of cellulose acetate from royal palm tree agroindustrial waste*, J. Polym. Engin. Sci., (2018).
9. M. Mahalakshmi, S. Selvanayagam, S. Selvasekarapandian, V. Moniha, R. Manjuladevi, and P. Sangeetha, *Characterization of biopolymer electrolytes based on cellulose acetates with magnesium perchlorate ($Mg(ClO_4)_2$) for energy storage devices,* J. Sci.: Advan. Mater. Dev., (2019).
10. R. Aihemaitituoheti, N.A. Alhebshi, and T. Abdullah, *Effects of Precursors and Carbon Nanotubes on Electrochemical Properties of Electrospun Nickel Oxide Nanofibers-Based Supercapacitors*, J. Molec., 26 (2021), 5656.

11. M. Diantoro, E.I.S. Suci, N. Zahro, F. Abdulloh, T. Ahmad, dan C. Laemthong, *Modifikasi Selulosa Asetat dengan Oksida Logam (ZnO, TiO_2 dan SnO_2) Film Superkapasitor Simetrik*, MSOpen. (2019).
12. S.A. Al Kiey, and M.S. Hasanin, *Green and facile synthesis of nickel oxide-porous carbon composite as improved electrochemical electrodes for supercapacitor application from banana peel waste*, Environ Sci Pollut Res., 28 (2021), 66888–66900.
13. Y.H. Navale, S.T. Navale, I.A. Dhole, F.J. tadler, and V.B. Patil, *Specific capacitance, energy and power density coherence in electrochemically synthesized polyaniline-nickel oxide hybrid electrode*, J. Organ. Elect., 57 (2018), 110–117.
14. W.G. Nunes, L.M. Da Silva, R. Vicentini, B.G.A. Freitas, L.H. Costa, A.M. Pascon, et al., *Nickel oxide nanoparticles supported onto oriented multi-walled carbon nanotube as electrodes for electrochemical capacitors*, J. Elect. Acta., 298 (2019), 468–483.
15. P. Wang, H. Zhou, C. Meng, Z. Wang, K. Akhtar, and A. Yuan, *Cyanometallic framework-derived hierarchical Co_3O_4-NiO/graphene foam as high-performance binder-free electrodes for supercapacitors*, J. Chem. Engin., 369 (2019), 57–63.
16. H. Doh, D.D. Kyle, and W. Scott, *Preparation of Novel Seaweed Nanocomposite Film from Brown Seaweeds Laminaria Japonica and Sargassum Natans*, J. Food Hydro., 105 (2020), 105744.
17. J. Basmal, I. Munifah, M. Rimmer and N. Paul, *Identification and characterization of solid waste from Gracilaria sp. extraction*, IOP Conf. Ser.: Earth Environ. Sci., 404 (2019), 012057.
18. P. Fei, L. Liao, B. Cheng, and J. Song, *Quantitative analysis of cellulose acetate with a high degree of substitution by FTIR and its application*, J. Analy. Metho., 9 (2017), 6194–6201.
19. Yusnimar, Evelyn, A. Aman, Chairul, S. Rahmadahana, and A. Amri, *Manufacturing of high brightness dissolving pulp from sansevieria-trifasciata fiber by effective sequences processes*, Commun. Sci. Technol., 7(1) (2022), 45-49.
20. H.M. Shaikh, A. Anis, A.M. Poulose, S.M. Al-Zahrani, N.A. Madhar, A. Alhamidi, et al., *Synthesis and Characterization of Cellulose Triacetate Obtained from Date Palm (Phoenix dactylifera L.) Trunk Mesh-Derived Cellulose*, J. Molec., 27 (2022), 1434.
21. S.T.C.L. Ndruru, D. Wahyuningrum, B. Bundjali, and I.M. Arcana, *Green simple microwave-assisted extraction (MAE) of cellulose from theobroma Cacao L. (TCL) Husk*, IOP Conf. Ser.: Mater. Sci. Eng., 541 (2019), 1-13.
22. D. Umaningrum, D.A. Maria, N. Radna, H. Hasanuddin, M. Ani, and M. Diah, *Variation of Iodine Mass and Acetylation Time On Cellulose Acetate Synthesis From Rice Straw*, Indo. J. Chem. Res., 8 (2021), 228-233.
23. R. Andalia, J. Rahmi, dan H. Hira, *Isolation and characterization of cellulose from ricehusk waste and sawdust with chemical method*, J. Natur., 20 (2020).
24. F. Meng, G. Wang, X. Du, Z. Wang, S. Xu, and Y. Zhang, *Preparation and characterization of cellulose nanofibers and nanocrystals from Liquefied Banana Pseudo-Stem Residue*, Compos. Part B.: Engi., 160 (2018), 341-347.
25. Rahmayetty, and F. Sulaiman, *Wastewater from the Arenga Starch Industry as a Potential Medium for Bacterial Cellulose and Cellulose Acetate Production*, J. Polym., 15 (2023), 870.
26. Y. Liu, S. Jiang, W. Yan, M. He, J. Qin, S. Qin, et al., *Crystallization Morphology Regulation on Enhancing Heat Resistance of Polylactic Acid*, J. Polym., 12 (2020), 1563.
27. S.E.I. Suryani, U. Sa'adah, W.N.L. Amini, T. Suprayogi, A.A. Mustikasari, A. Taufiq, et al., *Effect of ZnO and Annealing on the Hydrophobic Performance of x(ZnO)-CA-PLA*, J. Phys. Conf. Ser., 1093 (2018), 012003.
28. B. Delattre, R. Amin, J. Sander, J. De Coninck, A. P. Tomsia, and Y. M. Chiang, Impact of Pore Tortuosity on Electrode Kinetics in Lithium Battery Electrodes: Study in Directionally Freeze-Cast LiNi0.8Co0.15Al0.05O2(NCA), J. Elect. Socie., 165(2) (2018), A388–A395.
29. M. Diantoro, A.A. Mustikasari, N. Wijayanti, C. Yogihati, and A. Taufiq, *Microstructure and dielectric properties of cellulose acetate-ZnO/ITO composite films based on water hyacinth*, J. Phys. Conf. Ser., 853 (2017), 012047.
30. J. Fischer, K. Thümmler, S. Fischer, M.I.G. Gonzalez, S. Oswald, D. Mikhailova, *Activated Carbon Derived from Cellulose and Cellulose Acetate Microspheres as Electrode Materials for Symmetric Supercapacitors in Aqueous Electrolytes*, J. Energ. Fuel., 35 (2021), 12653–12665.
31. M.A. Teixeira, C.P Maria, P.A. Teresa, and P.F. Helena, *Electrospun Nanocomposites Containing Cellulose and Its Derivatives Modified with Specialized Biomolecules for an Enhanced Wound Healing*, J. nanomater., 19 (2020), 557.
32. E. Taer, Apriwandi, F. Hasanah, and R. Taslim, Nanofiber-enrich activated carbon coin derived from tofu dregs as electrode materials for supercapacitor, Commun. Sci. Technol., 6(1) (2021), 41-48.
33. H. Wei, H. Wang, A. Li, H. Li, D. Cui, M. Dong, et al., *Advanced porous hierarchical activated carbon derived from agricultural wastes toward high performance supercapacitors*, J. Alloy. Compoun., (2019), 153111.
34. E. Taer, L. Pratiwi, A. Apriwandi, W. S. Mustika, R. Taslim, and A. Agustino, Three-dimensional pore structure of activated carbon monolithic derived from hierarchically bamboo stem for supercapacitor application, Commun. Sci.Technol., 5(1) (2020), 22-30.